Liquid Crystals
Publication details, including instructions for authors and subscription information:
http://www.informaworld.com/smpp/title~content=t713926090

Influence of the thickness of a Ni x O y support on the reflected wavelength from cholesteric liquid crystals

M. Koui; H. S. Karayannis; M. Kartsonakis

Online publication date: 06 August 2010

To cite this Article Koui, M. , Karayannis, H. S. and Kartsonakis, M.(1997) 'Influence of the thickness of a Ni x O y support on the reflected wavelength from cholesteric liquid crystals', Liquid Crystals, 22: 5, 567 — 574
To link to this Article: DOI: 10.1080/026782997208965
URL: http://dx.doi.org/10.1080/026782997208965

LIQUID CRYSTALS, 1997, VOL. 22, NO. 5, 567–574

Influence of the thickness of a Ni_xO_y support on the reflected wavelength from cholesteric liquid crystals

by M. KOUI*, H. S. KARAYANNIS and M. KARTSONAKIS
Chemical Engineering Department, Materials Science and Engineering Section,
National Technical University of Athens, Zografou Campus,
9 Iroon Polytechniou Str., Zografou 15773, Athens, Greece

(*Received 29 September 1996; accepted 19 December 1996*)

In previous work [1–4] we found, for the first time, that the selectively reflected light band from cholesteric liquid crystals depends on the physical sorption properties of their supports, and we now use them to differentiate nickel electrodeposits with different grained texture and Ni_xO_y with various thicknesses. The different nickel oxide thicknesses were prepared by dipping the nickel electrodeposit samples into H_2O_2 solution for different time intervals. The selectively reflected light measurements from using the above samples were compared to each other, as well as to those from samples not dipped in H_2O_2 solution. All the experimental results were correlated with the properties of the deposits, as well as with the results derived from SEM. It is concluded that cholesteric liquid crystals can provide an efficient technique to identify surfaces with different grained texture and thickness of formed oxide.

1. Introduction

It is known that the light band reflected by a Cholesteric Liquid Crystal (ChLC) is usually shifted to longer wavelengths as the temperature decreases [5–7] or the applied pressure increases [8–11]. Also, electric or magnetic fields [5–7, 12, 13] and small quantities of impurities [14] change their colour. This colour change is due to the influence of the above mentioned parameters upon the pitch [5–14]. The sensitivity of the colour change is extremely strong in the neighbourhood of the cholesteric to smectic phase transition [6–12].

In our previous work [1–4, 15] it was found that the reflected light band of ChLCs also depends on the physical sorption properties of the surfaces of their supports. Therefore, if solid sorbents with high physical adsorption abilities were used as supports for a ChLC, the selectively reflected light from the ChLC was affected [1–4, 15] since the sorbents act on the sorbates with strong mechanical and/or electrical forces, due to the applied pressure [8–11] or to an electric [5–7, 12, 13] field, respectively, imposed by the sorbents. This explanation was further studied, and based upon it we differentiated γ_1-Al_2O_3 from γ_2-Al_2O_3 electrolytically prepared [1–3], γ_1-Al_2O_3 prepared with different current densities [1–3], chemically and electrolytically prepared ZnO and Fe_3O_4 [1–3], copper mechanically cleaned and electroplated [1–3], and nickel electrodeposited with different orientations [15]. We also differentiated [4], *in situ*, marble from gypsum and $CaCO_3$ from inversion of gypsum. The validity of a linear relationship was also shown between the adsorption properties of the support and the shift of the selectively reflected wavelength from the ChLC spread on the surface [3].

In the present work, measurements of the selectively reflected light band (visible diffuse reflectance spectroscopy) were carried out by using the same cholesteric mixture as in our previous work [1–4, 15].

The cholesteric mixture was spread on the surface of nickel electrodeposits which had been dipped in H_2O_2 solution for different time intervals (different thicknesses of formed oxide) and on the surface of nickel electrodeposits which had not been dipped into the H_2O_2 solution.

The different surfaces so formed show different properties [16–18] (chemical reactivity, hardness, reflectance, and sorption abilities due to the texture axis, the grain size and the various thicknesses of the formed oxide). The aim of the present work was to identify surfaces with different grained textures and thicknesses of the formed oxide by means of liquid crystals. It should be noted that large or small thickness of oxide formed under such conditions are important because they may be used as catalysts, as well as components of ceramics and composite materials.

2. Experimental

2.1. *Materials, shape, dimensions and preparation of the samples*

The nickel electrodeposits were prepared [18] in a simple constant temperature bath of 1·22M $NiCl_2 \cdot 6H_2O$

*Author for correspondence.

0267–8292/97 $12·00

solution at 50°C under galvanostatic conditions. An anode cylinder (∅ 2·7 cm, height 22 cm) of pure nickel and a cathode consisting of a stable bronze disc (∅ 2·8 cm and 0·35 cm thickness) were used.

The bath was agitated by a mechanical stirrer (1200 rpm). The cathode was first treated with a 10% (w/v) nitric acid solution and then was mechanically treated with emergy paper 180 and 800 in order to avoid epitaxial phenomena [19], i.e. so that the substrate did not impose its crystal structure on that of the deposit.

The disc was fitted to the bronze cathodic electrode covered by teflon, in such a way that the dipped surface of the bronze disc had a 2·4 cm ∅. The experimental set up for the electrolysis is shown in figure 1.

The duration of electrolysis was calculated according to the current density and efficiency in order to achieve about a 50 μm thickness of nickel electrodeposits. The electrolysis was carried out at pH = 3, which is the optimum pH value for nickel electrodeposition [16–20] and different samples were prepared using the following current densities: 15, 10, 5 and 2 A dm^{-2}.

2.2. *Experiments and experimental procedures*

The texture axis on all samples was identified by X-ray diffraction (XRD) analysis as shown in figure 2. The points marked 1–4 on the figure refer to the conditions of preparation of the nickel electrodeposited samples in the present work. The structure diagram of the electrodeposited samples is taken from our previous work [18].

Some of the nickel electrodeposits were kept in a dry environment and some of them were dipped in H_2O_2 solution (35% w/v) for intervals of 1, 3 and 6 days.

The examination of the sample surfaces was made using scanning electron microscopy (SEM) (Jeol Superprobe JXA-733). In figures 3–14, SEM photomicrographs are presented for all the samples, dipped and not dipped.

On the surface of all the samples 0·8 ml of the cholesteric mixture (1:4 ratio by wt. of cholesteryl-4carbomethoxyoxybenzoate and cholesteryl oleyl carbonate dissolved (10% w/v) in diethyl ether) was spread from a syringe, in order to ensure the same thickness (50–60 μm) of the mixture after evaporation of the diethyl ether.

The complete evaporation of the diethyl ether was assured by heating the samples (placed horizontally on

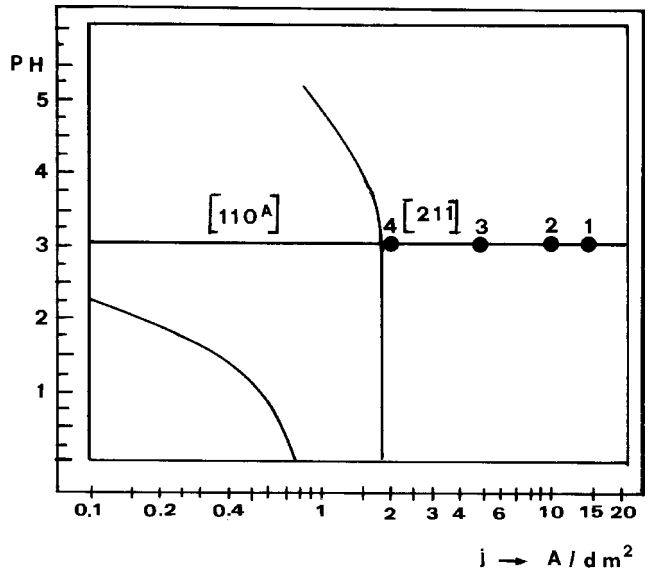

Figure 2. Regions of texture axes of the growth of Ni electrodeposits as a function of the current density and pH.

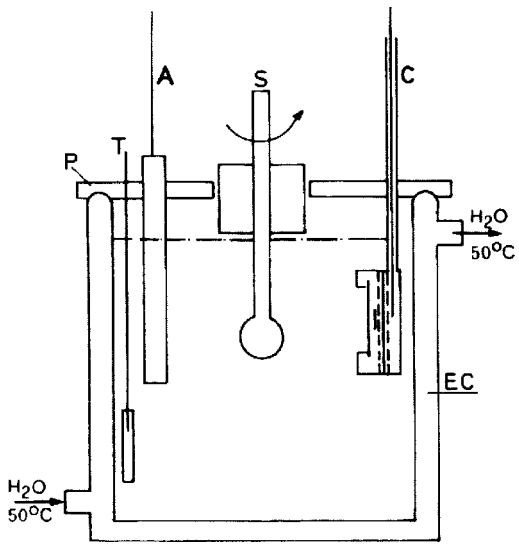

Figure 1. Schematic representation of the Ni electrodeposition set-up. EC: Electrolytic cell; P: plexiglass cover; T: thermometer; S: glass mechanical stirrer; A: anode Ni; C: cathode.

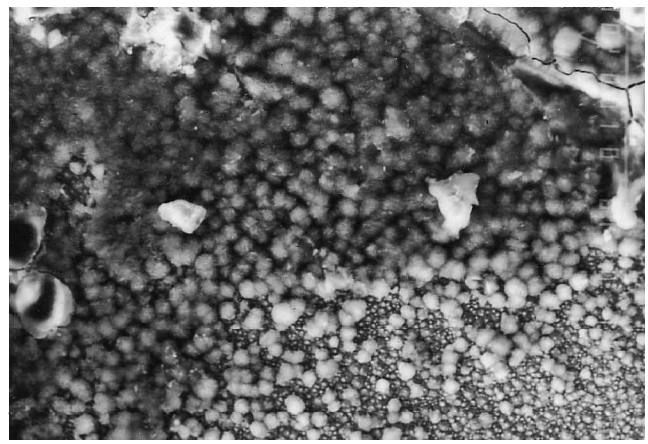

Figure 3. Non-dipped samples of the series 1, SEI × 300. Fine grained material (Ni electrodeposit).

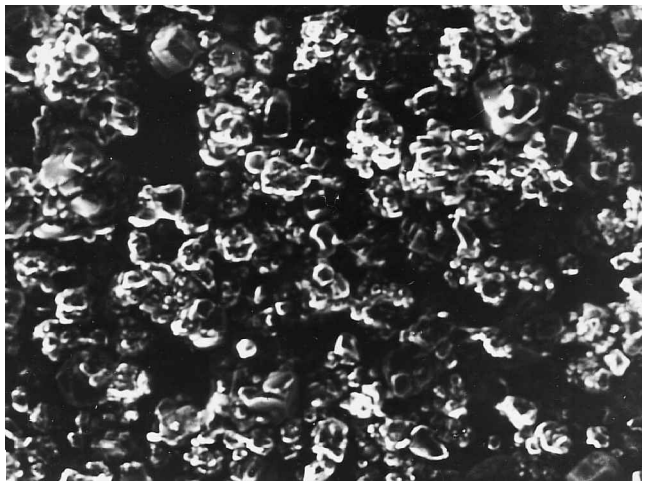

Figure 4. Non-dipped samples of the series 2, SEI × 250. Semi-fine grained material (Ni electrodeposit).

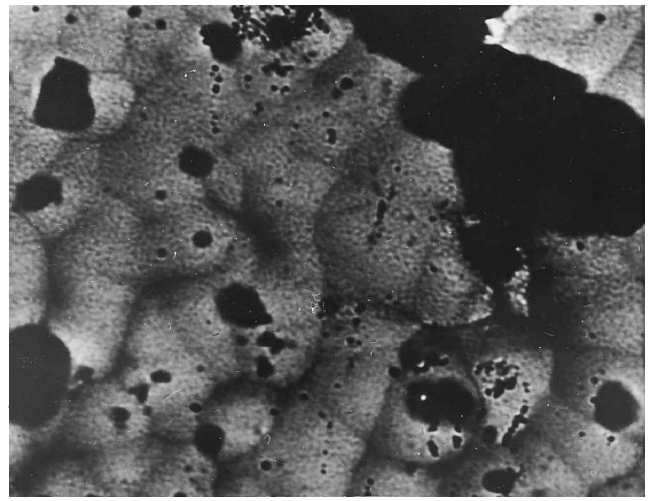

Figure 6. Non-dipped samples of the series 4, SEI × 250. Coarse grained material (Ni electrodeposit).

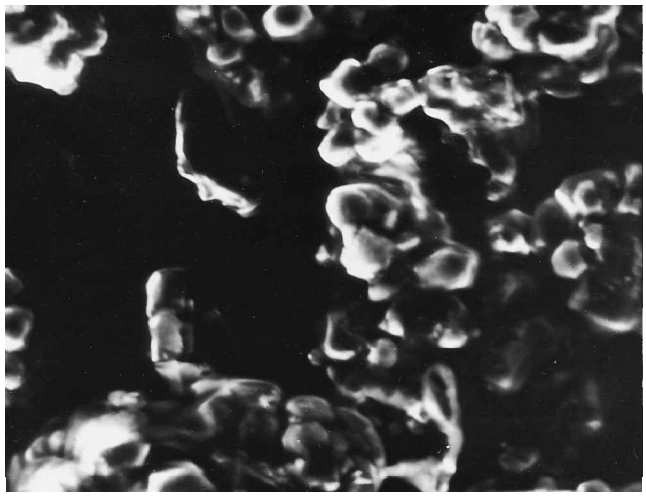

Figure 5. Non-dipped samples of the series 3, SEI × 250. Semi-coarse grained material (Ni electrodeposit).

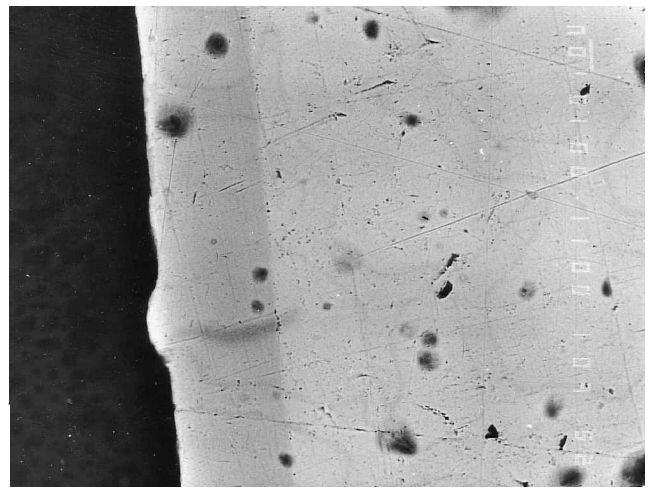

Figure 7. Section of a sample of the series 1, dipped for 3 days, BEI Compo × 400.

a thermostated plate) above the isotropic (35°C) transition point. Then the sample was allowed to cool and manipulated mechanically in order to acquire the Grandjean microstructure.

From all the types of samples, visible diffuse reflectance spectra [3] at the temperatures 25, 26, 27 and 28°C were taken after covering the surface with the cholesteric mixture. For the measurements, a Perkin-Elmer double beam spectrophotometer (mod. Lamda 3 UV/VIS) for visible light with an integrating sphere attachment (Perkin Elmer Type R 453) was used. Each sample with the cholesteric mixture, treated as mentioned above, was placed on a special thermostated block-heater and introduced into the apparatus (in the compartment designed for back reflection measurements) lying normal to the light beam. Spectra were taken at the above mentioned constant temperatures with an accuracy of $\pm 0{\cdot}1$°C. The accuracy of the wavelength measurements was $\pm 0{\cdot}5$ nm. Measurements were taken on six samples of each series at each temperature, and the mean value (λ) was calculated in nm. The derived results are shown in tables 1, 2, 3 and 4 and in figures 15–18.

3. Results and discussion

Results derived from spectral measurements (table 1, figure 15) reveal different shifts of the reflected light band from the cholesteric mixture between the samples not dipped in H_2O_2 solution. Comparing the results between the rows of table 1, from series 1 to 4, it is observed that as the current density decreases the shift of the selectively reflected wavelength increases.

Furthermore, as shown in figures 3–6, relating to

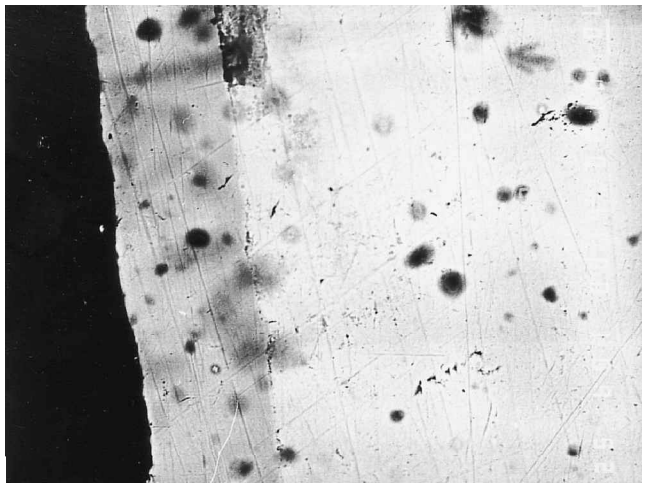

Figure 8. Section of a sample of the series 2, dipped for 3 days, BEI Compo × 400.

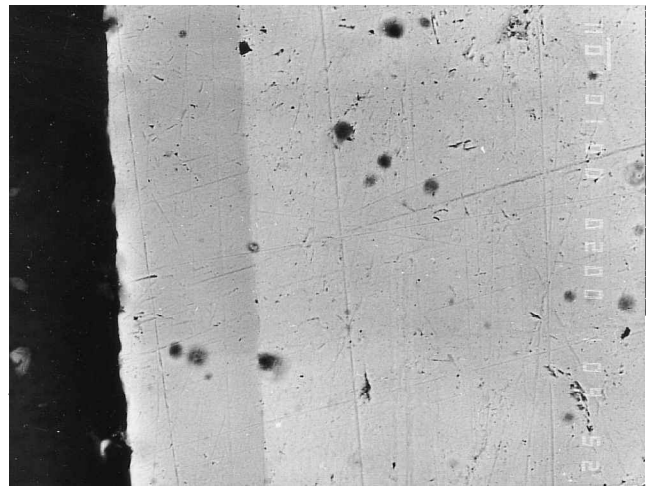

Figure 10. Section of a sample of the series 4, dipped for 3 days, BEI Compo × 400.

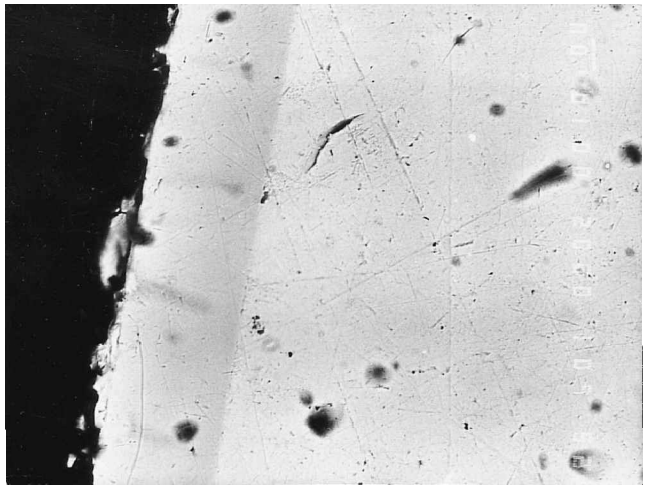

Figure 9. Section of a sample of the series 3, dipped for 3 days, BEI Compo × 400.

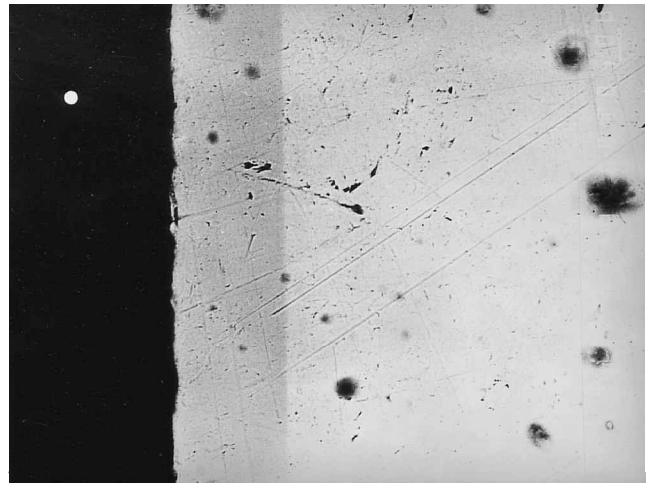

Figure 11. Section of a sample of the series 1, dipped for 6 days, BEI Compo × 400.

SEM analysis of the surfaces of these samples, the textures of the deposits range from quasi-porous to those of a compact material of pyramidic structure. As current density increases, the crystallites become finer and the material appears more compact [18]. Figure 3, relating to the samples of series 1 prepared with the highest current density, presents a fine pyramidic development of the crystallites with some tendency to become spheroidised. This may be attributed to a high relative rate of H_2 evolution under the Ni-deposit preparation conditions [18]. At lower current density (samples of series 2), the grains observed are larger, better organized and the pyramidic structure starts to be more concrete (figure 4). As the current density is reduced (samples of series 3), the crystallites presented are substantially bigger, the agglomerates are better formed and a clear dendritic structure is observed (figure 5). In figure 6, relating to the lowest current density (samples of series 4), the material consists of coarse spheroidised/pyramidic grains. Densely packed grains produce big agglomerates with a linear arrangement forming columns. The black areas or 'craters' observed on the surface of pyramids are holes formed by small hydrogen bubbles absorbed during the formation of Ni-deposits. In the lower region of figure 6 the boundaries between two neighbouring coarse pyramids are shown.

The observations derived from SEM analysis combined with the spectral measurements (table 1, figure 15) suggest that the different shifts of the reflected light band from the cholesteric mixture can be attributed to the size and the shape of the crystallites of the Ni-deposits. Therefore, as the current density increases, the material

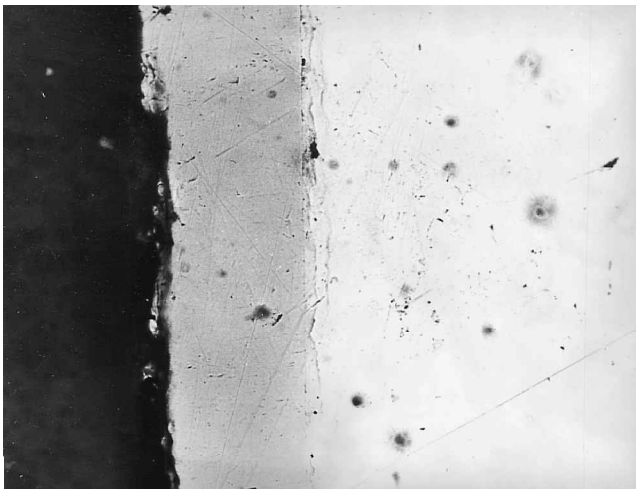

Figure 12. Section of a sample of the series 2, dipped for 6 days, BEI Compo × 400.

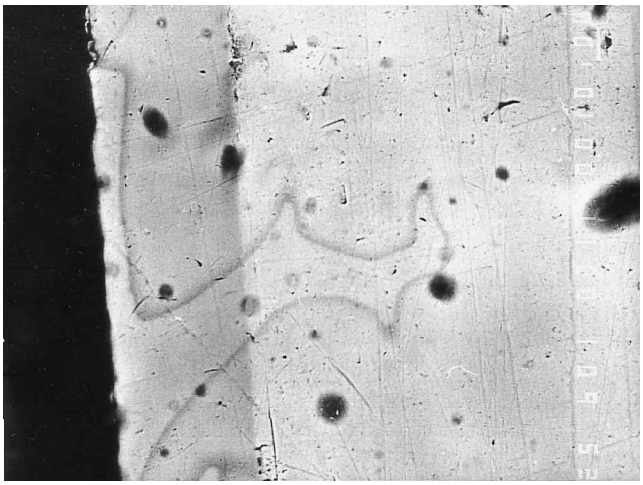

Figure 13. Section of a sample of the series 3, dipped for 6 days, BEI Compo × 400.

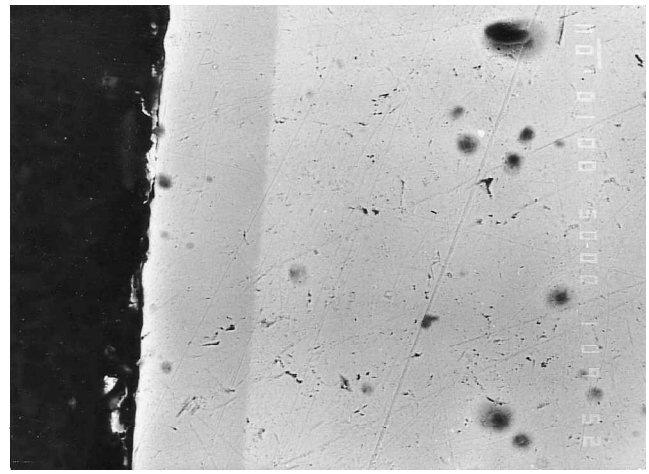

Figure 14. Section of a sample of the series 4, dipped for 6 days, BEI Compo × 400.

Table 1. Non-dipped samples; mean λ/nm.

		Temperature/°C			
Sample series	Current density/A dm^{-2}	25	26	27	28
1 [211]	15	520	458	430	416
2 [211]	10	528	465	435	420
3 [211]	5	534	470	442	424
4 [211]	2	545	478	447	432

becomes finer and more compact and the shift of the selectively reflected wavelength decreases.

For the series of samples dipped in H_2O_2 solution (tables 2, 3, 4) such a comparison is not possible, because each series has a different behaviour in the H_2O_2 solution, even for the same period of exposure. Furthermore, the growth of oxide formed is different for each series of samples due to their microstructural differences.

From tables 2, 3 and 4, the respective figures 16–18 and the SEM photomicrographs (figures 7–14), it is observed that different thicknesses of the nickel oxide lead to different shifts of the selectively reflected wavelength band of the cholesteric mixture.

In all the figures 7–14, the darker zone appearing between the black and the light parts of the photomicrographs is the cross-section of the nickel oxide zone, corresponding to the thickness of the formed nickel oxide. In all cases the appearance of the oxide was dark grey, while the nickel electrodeposit always had a colour ranging from light grey up to grey.

Thus, all the results reveal the high sensitivity of this method, particularly in the cases mentioned above relating to the texture axis and the oxide thickness which impose different properties such as reflectance, hardness, rate of reaction, catalytic properties [16–18, 21] and sorption abilities.

The samples of series 1, prepared at c.d. = 15 A dm^{-2} give the maximum thickness when dipped in the H_2O_2 solution for 1 day. For 3 and 6 days' dipping, the thickness of the oxide is reduced, because of oxide dissolution in the H_2O_2 solution (figures 7 and 11). These observations are supported by the fact that the electrolysis conditions (pH, c.d., etc.) lead to a deposit with a texture axis [2 1 1] sensitive to oxidation. That is why the selectively reflected wavelength is considerably longer for the samples dipped in H_2O_2 solution for 1 day than for those dipped for 3 and 6 days (tables 2, 3, 4 and figures 16, 17, 18).

The samples of the series 2, prepared at a c.d. = 10 A dm^{-2}, formed the thickest oxide. The thickness of the oxide increases as dipping time increases, so the

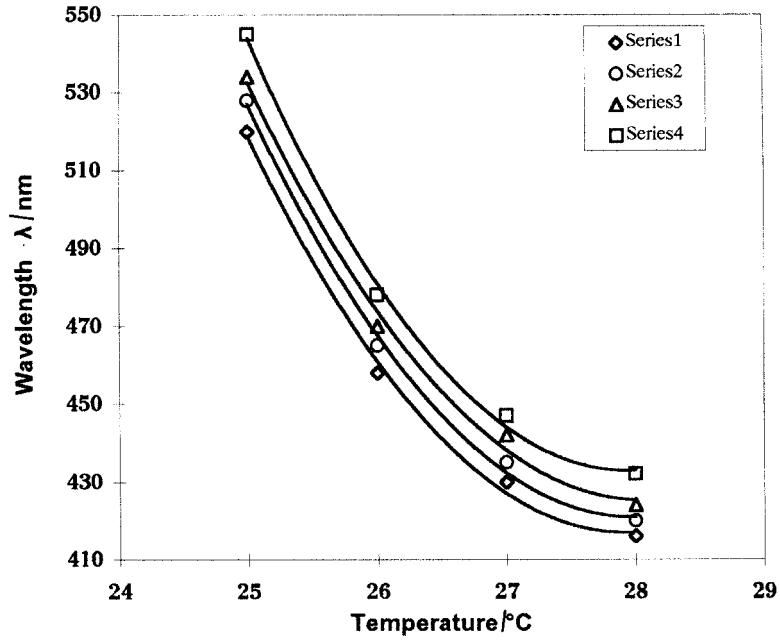

Figure 15. Shift of the selectively reflected wavelength λ (nm) vs. temperature for all non-dipped samples of series 1–4. (1) 15 A dm^{-2}, (2) 10 A dm^{-2}, (3) 5 A dm^{-2}, (4) 2 A dm^{-2}.

Table 2. Dipped samples for 1 day; mean λ/nm.

		Temperature/°C			
Sample series	Current density/Adm^{-2}	25	26	27	28
1 [211]	15	573	507	470	455
2 [211]	10	554	486	456	438
3 [211]	5	550	483	452	435
4 [211]	2	560	495	463	443

Table 3. Dipped samples for 3 days; mean λ/nm.

		Temperature/°C			
Sample series	Current density/Adm^{-2}	25	26	27	28
1 [211]	15	558	492	460	440
2 [211]	10	570	500	468	450
3 [211]	5	567	498	465	446
4 [211]	2	590	517	482	460

Table 4. Dipped samples for 6 days; mean λ/nm.

		Temperature/°C			
Sample series	Current density/Adm^{-2}	25	26	27	28
1 [211]	15	549	480	449	430
2 [211]	10	615	540	498	470
3 [211]	5	596	523	486	462
4 [211]	2	553	486	455	436

maximum thickness is reached on the sixth day (tables 2, 3, 4 and figures 8, 12, 16, 17, 18).

A similar behaviour to that of the above series of samples series 2 is observed for samples of series 3 prepared at a c.d.$=5$ A dm^{-2}. Again, the thickest oxide layer is attained on the sixth day, but without achieving the same thickness (figures 12 and 13). This is revealed by the fact that the selectively reflected wavelength on the sixth day is clearly shorter than that of the sample of series 2 (tables 2, 3, 4 and figures 16, 17, 18).

Samples of both series 2 and 3 have the same secondary structure [2 1 1]. The observed differences of their oxidation behaviour (i.e. different thicknesses of the formed oxide) are due to the different perfection of the texture axis. The texture axis of series 2 is more perfect than that of series 3, because [2 1 1] is a texture axis which has been prepared under such conditions [22] that inhibition of crystallization is weaker. Therefore, the crystallites of the deposits of series 2 are better organized than those of the series 3.

Thus, it is suggested that the cholesteric liquid crystals method can be an efficient technique to distinguish different thicknesses of the formed oxide layers.

The samples of the series 4, prepared at a c.d.$=$ 2 A dm^{-2}, reach a maximum oxide layer thickness after 3 days' dipping (figure 10). This sample series presents a smaller thickness of the oxide layer formed compared with series 2 and 3 (figures 8–10, 12–14). This behaviour is attributed to the microstructure of the formed electrodeposits, which have been prepared at the transition point of the texture axis $[1\,1\,0]^{A} \rightarrow [2\,1\,1]$ as shown in figure 2. Thus, a part of the microstructure consists of the microstructural characteristics of texture axis $[1\,1\,0]^{A}$ that is a fine spongy material [18]. The lower value of the selectively reflected wavelength for six days'

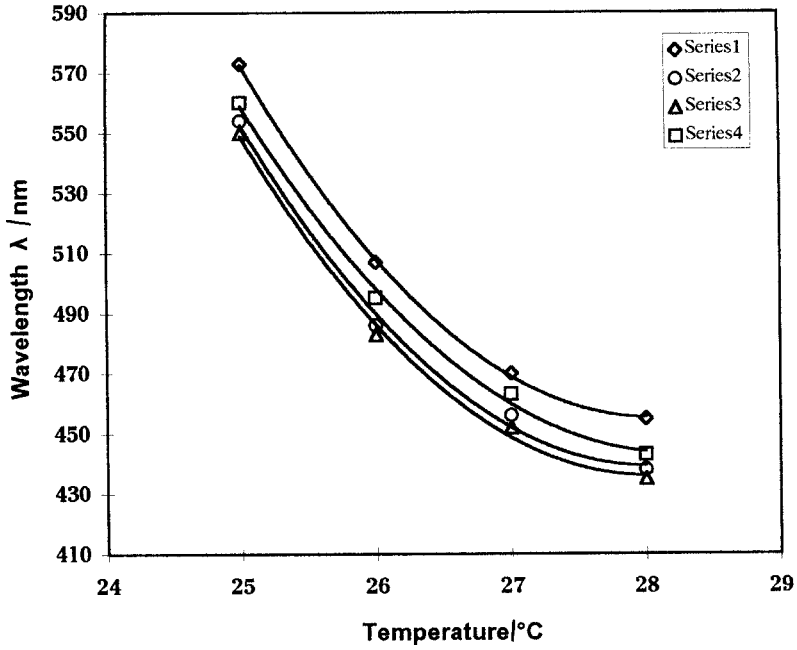

Figure 16. Shift of the selectively reflected wavelength λ (nm) vs. temperature for all dipped samples of series 1–4 for one day. (1) 15 A dm^{-2}, (2) 10 A dm^{-2}, (3) 5 A dm^{-2}, (4) 2 A dm^{-2}.

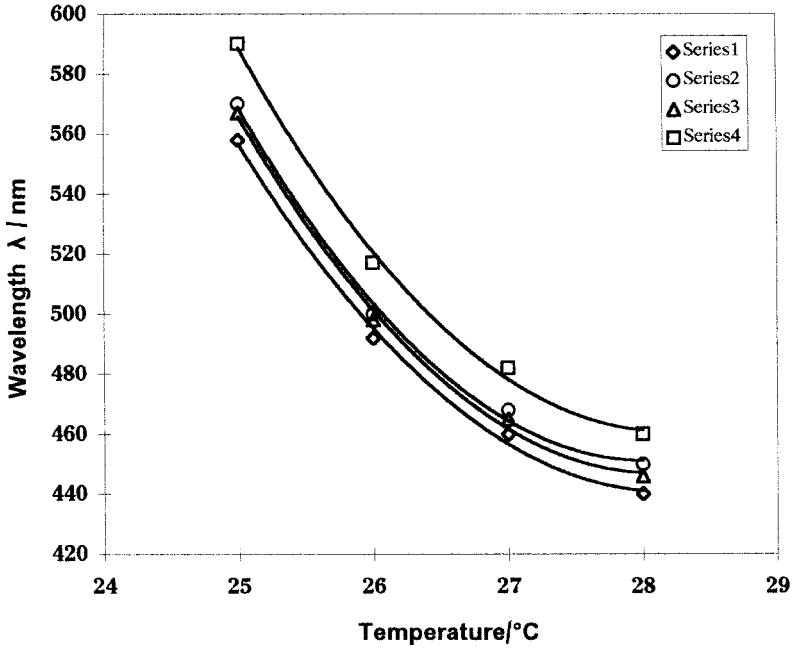

Figure 17. Shift of the selectively reflected wavelength λ (nm) vs. temperature for all dipped samples of series 1–4 for 3 days. (1) 15 A dm^{-2}, (2) 10 A dm^{-2}, (3) 5 A dm^{-2}, (4) 2 A dm^{-2}.

dipping is due to the dissolution of the formed oxide in the H_2O_2 solution (tables 2, 3, 4 and figures 16, 17, 18).

Comparing the samples not dipped in H_2O_2 (figures 3–6), it is observed that the surface of each sample is different because of the different size of the crystal grains [18] (crystallites). From table 1 and figure 15 it is revealed that an increase of crystallite size leads to longer wavelengths of the selectively reflected light from the cholesteric mixture.

Thus, the extreme sensitivity of this method is revealed, and therefore it is suggested as an appropriate technique to distinguish crystallites of different size (fine grained, medium grained, coarse grained samples). It must be noted that the usual method using physical sorption of methylene blue is not sensitive enough to maintain such a differentiation, and even in cases that measurements are feasible the extremely small quantities of methylene blue absorbed result in poor accuracy.

4. Conclusions

The results derived from the present research lead to the following conclusions:

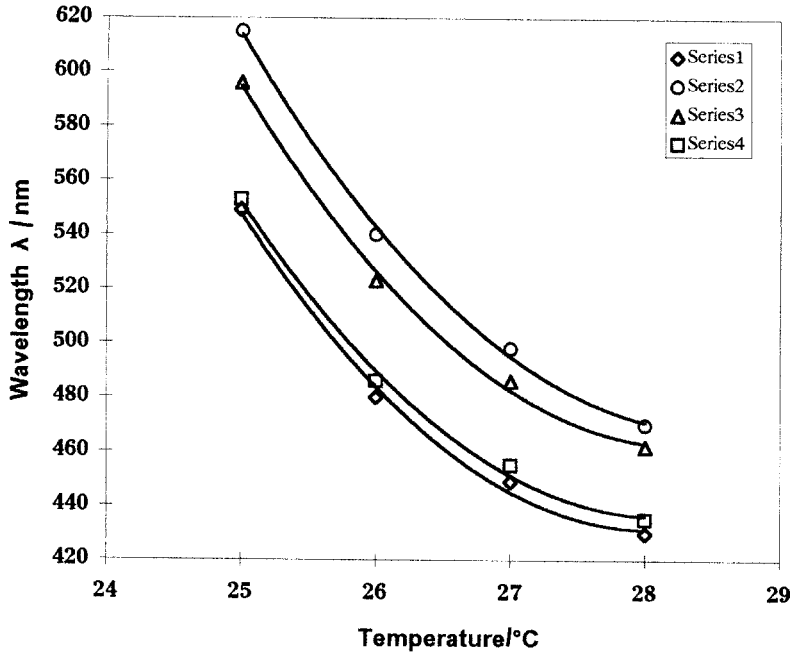

Figure 18. Shift of the selectively reflected wavelength λ (nm) vs. temperature for all dipped samples of series 1–4 for 6 days. (1) 15 A dm^{-2}, (2) 10 A dm^{-2}, (3) 5 A dm^{-2}, (4) 2 A dm^{-2}.

(1) The selectively reflected light from a cholesteric mixture shifts to longer wavelengths as the sorption abilities of the solid support increase, confirming the suggestions reported in our previous work [1–4].

(2) Cholesteric liquid crystals provide an efficient technique to identify surfaces of different grained texture and thickness of the formed oxide with high accuracy, even in cases where direct sorption measurements are not feasible.

(3) The differentiation is enhanced as the temperature decreases.

In addition, the conclusions derived concerning differentiation of the grained texture and the thickness of the nickel oxide formed suggest that the cholesteric mixture spread on oxidised metal surfaces may be used further to provide information on the type and the intensity of oxidation.

References

[1] Skoulikidis, Th., and Koui, M., 1980, *Mol. Cryst. liq. Cryst.*, **61,** 31.
[2] Skoulikidis, Th., and Koui, M., 1981, *Scuola sui Cristalli Liquidi, UNICAL-81*, University of Calabria, Italy.
[3] Skoulikidis, Th., and Koui, M., 1983, *Mol. Cryst. liq. Cryst.*, **95,** 323.
[4] Skoulikidis, Th., Koui, M., and Kostoudi, A., 1991, *Mol. Cryst. liq. Cryst.*, **206,** 117.
[5] DeGennes, P. G., 1974, *The Physics of Liquid Crystals* (Oxford: Clarendon Press).
[6] Brown, G. H., 1976, *Advances in Liquid Crystals*, Vol. 2, (New York: Academic Press).
[7] Brown, G. H., 1977, *J. Colloid interface Sci.*, **58,** 534.
[8] Kayes, P. H., Weston, H. T., and Daniels, W. B., 1973, *Phys. Rev. Lett.*, **31,** 628.
[9] Polmann, P., and Stegemeyer, H., 1974, *Ber. Bunsenges. phys. Chem.*, **78,** 843.
[10] Polmann, P., 1974, *Ber. Bunsenges. phys. Chem.*, **78,** 374.
[11] Polmann, P., 1974, *J. Phys. E sci. Instrum.*, **7,** 490.
[12] Meier, G., Sackmann, E., and Gradmaier, J. G., 1975, *Applications of Liquid Crystals* (Berlin: Springer-Verlag).
[13] Khoo, I.-C., and Wu, S.-T., 1993, *Optics and Nonlinear Optics of Liquid Crystals*, Vol. VI (Singapore: World Scientific Publications).
[14] Gray, G. W., and Winsor, P. A., (editor) 1974, *Liquid Crystals and Plastic Crystals* (Chichester: Ellis Horwood Ltd).
[15] Skoulikidis, Th., Polymenis, S., and Kostoudi, A., 1988, *Mol. Cryst. liq. Cryst.*, **158,** 197.
[16] Amblard, J., Froment, M., and Spyrellis, N., 1977, *Surf. Technol.*, **5,** 205.
[17] Karayannis, H. S., 1986, *Chim. Chron. (Greece) B.*, 642.
[18] Karayannis, H. S., and Patermarakis, G., 1995, *Electrochem. Acta V*, **40,** 1079–1092.
[19] Maurin, G., 1970, *Oberflache-Surface*, **11,** 297.
[20] Maurin, G., 1971, *Oberflache-Surface*, **12,** 8.
[21] Brenner, A., and Jennings, C. W., 1948, *Plating*, **35,** 452.
[22] Spyrellis, N., Amblard, J., Froment, M., and Maurin, G., 1987, *J. Micros. Spectrosc. Electron*, 221.